Neutralino dark matter and other LHC predictions from quasi Yukawa unification

Qaisar Shafi [a], Şükrü Hanif Tanyıldızı [b], Cem Salih Ün [c,*]

[a] *Bartol Research Institute, Department of Physics and Astronomy, University of Delaware, Newark, DE 19716, USA*
[b] *Bogoliubov Laboratory of Theoretical Physics, Joint Institute for Nuclear Research, 141980 Dubna,
Moscow Region, Russia*
[c] *Department of Physics, Uludağ University, Bursa TR16059, Turkey*

Abstract

We explore the dark matter and LHC implications of $t - b - \tau$ quasi Yukawa unification in the framework of supersymmetric models based on the gauge symmetry $G = SU(4)_c \times SU(2)_L \times SU(2)_R$. The deviation from exact Yukawa unification is quantified by a dimensionless parameter C ($|C| \lesssim 0.2$), such that the Yukawa couplings at M_{GUT} are related by $y_t : y_b : y_\tau = |1 + C| : |1 - C| : |1 + 3C|$. In contrast to earlier studies which focused on universal gaugino masses, we consider non-universal gaugino masses at M_{GUT} that are compatible with the gauge symmetry G. Our results reveal a variety of neutralino dark matter scenarios consistent with the observations. These include stau and chargino coannihilation scenarios, the A-resonance scenario, as well as Higgsino dark matter solutions which are more readily probed by direct detection searches. The gluino mass is found to be $\lesssim 4$ TeV, the stop mass is $\gtrsim 2$ TeV, while the first two family squarks and sleptons are of order 4–5 TeV and 3 TeV respectively.

* Corresponding author.
  E-mail addresses: shafi@bartol.udel.edu (Q. Shafi), hanif@theor.jinr.ru (Ş.H. Tanyıldızı),
cemsalihun@uludag.edu.tr (C.S. Ün).

1. Introduction

In an earlier paper [1], we have explored the LHC implications of imposing $t - b - \tau$ Quasi-Yukawa Unification (QYU) at the grand unification scale ($M_{\text{GUT}} \sim 2 \times 10^{16}$ GeV). This modified approach to the third family ($t - b - \tau$) YU [2] can be motivated by the desire to construct realistic supersymmetric models of grand unified theories (GUTs) which also incorporate realistic masses and mixings observed in the matter sector. For instance, the desired quark and charged lepton masses for the second family fermions can be incorporated, following [3], by including Higgs fields in $H'(15, 1, 3)$ representation of $G = SU(4)_c \times SU(2)_L \times SU(2)_R$ (hereafter 4-2-2) [4], which develops a non-zero GUT scale vacuum expectation values (VEVs). The third family Yukawa couplings receive, in this case, sizable new contributions, and the deviations from exact YU can be stated as follows [1]:

$$y_t : y_b : y_\tau = \mid 1 + C \mid : \mid 1 - C \mid : \mid 1 + 3C \mid \tag{1}$$

where C measures the deviation from the exact YU. Restricting the deviation to $\mid C \mid \lesssim 0.2$ we refer Eq. (1) to QYU condition. Note that C can be taken positive by appropriately adjusting the phases of the Higgs fields H and H' [3].

The 4-2-2 model has many salient features distinguishing it from other high scale theories [5]. The discrete left–right (LR) symmetry reduces the number of gauge couplings from three to two with $g_L = g_R$. It also requires gaugino masses of $SU(2)_L$ and $SU(2)_R$ to be equal at M_{GUT}. Furthermore, if 4-2-2 breaks into MSSM at around the GUT scale, the threshold corrections to the gauge couplings become negligible and unification of MSSM gauge couplings is approximately maintained. If one assumes the underlying GUT symmetry is $SO(10)$, in the breaking pattern, the 16-plet of SO(10) splits into $\psi(4, 2, 1)$ and $\psi_c(\overline{4}, 2, 1)$ under 4-2-2. Using left–right symmetry, the soft masses associated with ψ and ψ_c are equal. In addition, the LR symmetry requires the existence of right-handed neutrino. However, if the Dirac Yukawa coupling associated with the right-handed neutrino is adequately small [6], its contribution to the low scale supersymmetric phenomenology is negligible, and hence we do not include it in our study.

In this paper we reconsider QYU in the framework of 4-2-2 defined above, taking into account the fact that the MSSM gaugino masses $M_{1,2,3}$ at M_{GUT} can be non-universal. In particular, we assume the following asymptotic relation [7]

$$M_1 = \frac{3}{5}M_2 + \frac{2}{5}M_3 \;\;, \tag{2}$$

which follows from the assumption of left–right symmetry at M_{GUT} and the fact that $U(1)_Y$ derived from 4-2-2 is given as follows:

$$Y = \sqrt{\frac{3}{5}}I_{3R} + \sqrt{\frac{2}{5}}(B - L). \tag{3}$$

Here M_1, M_2 and M_3 are the asymptotic gaugino masses for $U(1)_Y$, $SU(2)_L$ and $SU(3)_c$, and I_{3R} and $(B - L)$ are diagonal generators of $SU(2)_R$ and $SU(4)_c$ respectively. Note that either M_2 or M_3 can have a positive sign by convention, while the other has a freedom to be negative. Previous studies [8,9] have shown that the 4-2-2 setup with opposite sign gaugino masses leads to a fairly rich phenomenology even if exact Yukawa unification (i.e. $C = 0$) is imposed. For instance, Yukawa unification can be achieved at low values of m_{16} (~ 800 GeV) in contrast to other Yukawa unified models which predict Yukawa unification for $m_{16} \gtrsim 8$ TeV [7]. Besides, there are a variety of coannihilation channels consistent with Yukawa Unification which reduce

the LSP neutralino relic density to the ranges consistent with the WMAP bound. Considering QYU in this case does not significantly change the low scale phenomenology. On the other hand, the case of 4-2-2 with positive gaugino masses provides a very stringent framework if exact Yukawa unification is imposed. Despite a variety of coannihilation channels [10], only the gluino–neutralino coannihilation can survive under the Yukawa unification condition [7]. Relaxing $t - b - \tau$ Yukawa Unification to $b - \tau$ Yukawa Unification allows, in addition, the stop–neutralino coannihilation channel [11]. In this respect, QYU leads to a very different low scale phenomenology with all gaugino masses positive. Therefore we restrict ourselves in our study to the case in which the gauginos all have positive masses.

The setup of our paper is as follows. In Section 2 we briefly explain our scanning procedure and list the experimental constraints that we impose on the data obtained from our scans. In Section 3 we show the fundamental parameter space that is allowed by the experimental constraints and QYU. Section 4 provides the implications for dark matter sector such as coannihilation channels and the resonance solution. Section 5 considers a Higgsino-like LSP and we emphasize the implications for direct detection experiments. We also present the benchmark points to exemplify our results. We conclude our study in Section 6.

2. Scanning procedure and experimental constraints

In our scan, we employ ISAJET 7.84 [12] to calculate the low scale observables. The gauge and Yukawa couplings are first estimated at the low scale. ISAJET evolves the gauge couplings and the Yukawa couplings of the third family up to M_{GUT}. We do not strictly enforce the gauge unification condition $g_1 = g_2 = g_3$, since a few percent deviation from the gauge coupling unification can be generated by unknown GUT-scale threshold corrections [13]. Hence, M_{GUT} is calculated to be the scale where $g_1 = g_2$ and g_3 deviates a few percent. After M_{GUT} is determined, the soft supersymmetry breaking (SSB) parameters determined with the boundary conditions defined at M_{GUT} are evolved together with the gauge and Yukawa couplings from M_{GUT} to the weak scale M_Z.

The SUSY threshold corrections to the Yukawa couplings [14] are taken into account at the common scale $M_{\mathrm{SUSY}} = \sqrt{m_{\tilde{t}_L} m_{\tilde{t}_R}}$. The entire parameter set is iteratively run between M_Z and M_{GUT} using full 2-loop RGEs, and the SSB parameters are extracted from RGEs at the appropriate scales $m_i = m_i(m_i)$.

We have performed random scans over the following parameter space:

$$0 \leq m_{16} \leq 10\,000 \text{ GeV}$$
$$0 \leq M_2 \leq 2000 \text{ GeV}$$
$$0 \leq M_3 \leq 2000 \text{ GeV}$$
$$-3 \leq A_0/m_{16} \leq 3$$
$$40 \leq \tan\beta \leq 60$$
$$0 \leq m_{10} \leq 10\,000 \text{ GeV}$$
$$\mu > 0, \qquad m_t = 173.3 \text{ GeV}. \tag{4}$$

Considering the similarities between $SO(10)$ and the Pati–Salam gauge group with imposed LR symmetry discussed above, we use the $SO(10)$ notation to describe the boundary conditions compatible with 4-2-2. In this context, m_{16} defines the universal SSB terms for the matter fields, and m_{10} stands for the universal SSB mass term for the MSSM Higgs doublets. M_2, M_3 are the SSB

mass terms for the gauginos of $SU(2)_L$ and $SU(3)_c$ respectively, and M_1 is determined asymptotically in terms of M_2 and M_3 as given in Eq. (2). A_0 is the universal SSB term for trilinear scalar interactions, $\tan\beta$ is the ratio of VEVs of the MSSM Higgs doublets, μ is coefficient of the bilinear Higgs mixing term, and m_t is the top quark mass. Note that we set the top quark mass to 173.3 GeV [15,16], and our results are not too sensitive to a $1\sigma - 2\sigma$ variation in m_t [17].

We employ the Metropolis–Hastings algorithm as described in [18], and require all collected points to satisfy radiative electroweak symmetry breaking (REWSB) with LSP neutralino. The REWSB gives a crucial theoretical constraint on the parameter space [19]. After collecting data, we impose constraints from the mass bounds [20], rare decays of B-meson such as $B_s \to \mu^+\mu^-$ [21], $b \to s\gamma$ [22], and $B_u \to \tau\nu_\tau$ [23]. After obtaining the region allowed by the LHC constraints, we also apply the WMAP bound [24] on the relic abundance of LSP neutralino. ISAJET interfaces with IsaTools [25,26] for B-physics and relic density observables. The experimental constraints imposed in our data can be summarized as follows:

$$m_h = (123 - 127) \text{ GeV}$$
$$m_{\tilde{g}} \geq 1.4 \text{ TeV}$$
$$0.8 \times 10^{-9} \leq \text{BR}(B_s \to \mu^+\mu^-) \leq 6.2 \times 10^{-9} \ (2\sigma)$$
$$2.99 \times 10^{-4} \leq \text{BR}(b \to s\gamma) \leq 3.87 \times 10^{-4} \ (2\sigma)$$
$$0.15 \leq \frac{\text{BR}(B_u \to \tau\nu_\tau)_{\text{MSSM}}}{\text{BR}(B_u \to \tau\nu_\tau)_{\text{SM}}} \leq 2.41 \ (3\sigma)$$
$$0.0913 \leq \Omega_{\text{CDM}}h^2 \leq 0.1363 \ (5\sigma). \tag{5}$$

We emphasize here the mass bounds on the Higgs boson [27,28] and gluino [29]. We allow a few percent deviation from the observed mass of the Higgs boson, since there exist about a 2 GeV error in estimation of its mass arising due to theoretical uncertainties in the calculation of the minimum of the scalar potential, and experimental uncertainties in m_t and α_s [30]. Besides these constraints, we require our solutions to do no worse than the SM in comparing predictions for the muon anomalous magnetic moment. Note that the WMAP bound on the DM relic density provides a very stringent constraint, since the relic density of LSP neutralino as a candidate for the DM can be very large over the parameter space. Moreover, as a solution of the Boltzmann equation, the relic density is in exponential form [31,32], and so even small deviations in model parameters can exponentially affect the results in calculation of the relic density. Additionally, one can also assume a multi-component DM scenario, and consider the LSP neutralino as one of the components. Such an assumption can relax the lower bound on the relic density which can alter the DM phenomenology, especially for the cases in which the LSP neutralino is Higgsino-like, or formed by bino–wino mixing. Even though we do not exclude such viable DM scenarios, we assume the DM relic density is saturated only by the LSP neutralino.

3. Fundamental parameter space of Quasi Yukawa Unification and sparticle mass spectrum

In this section we highlight the allowed regions in the fundamental parameter space of 4-2-2 given in Eq. (4) and present the results for the mass spectrum of colored supersymmetric particles. Fig. 1 shows the plots in C–m_{16}, C–m_{10}, C–M_2 and C–M_3 planes. All points are compatible with REWSB and LSP neutralino. Green points satisfy the mass bounds on the sparticles and the Higgs boson, and the constraints from rare B-decays. Blue points form a subset of green and
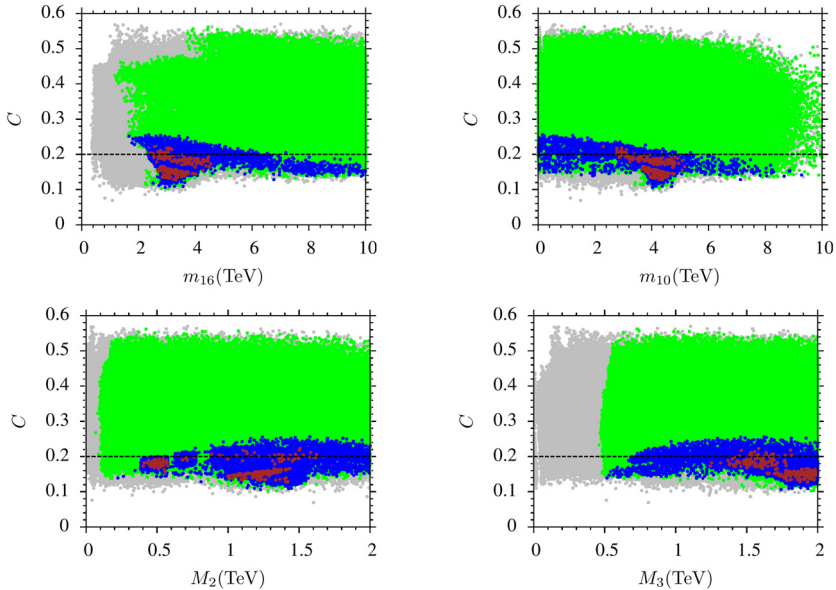
Fig. 1. Plots in $C-m_{16}$, $C-m_{10}$, $C-M_2$ and $C-M_3$ planes. All points are compatible with REWSB and LSP neutralino. Green points satisfy the mass bounds on the sparticles and the Higgs boson, and the constraints from rare B-decays. Blue points form a subset of green and they are compatible with the QYU condition. Note that we allow the solutions also for $C > 0.2$, since the vertical axis represents C itself. A dashed line indicating $C = 0.2$ has been used in these plots. Points in red form a subset of blue and satisfy the WMAP constraint on relic abundance of LSP neutralino. (For interpretation of the references to color in this figure legend, the reader is referred to the web version of this article.)

they are compatible with the QYU condition. Note that we allow the solutions also for $C > 0.2$, since the vertical axis represents C itself. A dashed line indicating $C = 0.2$ has been used in these plots. Points in red form a subset of blue and satisfy the WMAP constraint on relic abundance of LSP neutralino. As seen from the $C-m_{16}$ panels, QYU (blue) requires $m_{16} \gtrsim 2$ TeV. Even though it is possible to find solutions compatible with QYU for $m_{16} \sim 500$ GeV [1], such solutions have been excluded by the constraint from the Higgs boson mass. In contrast to m_{16}, m_{10} is only loosely constrained by QYU. As seen from the $C-m_{10}$ panel, it is possible to find solutions compatible with QYU (blue region) at any scale of m_{10}. However, it is constrained to $m_{10} \gtrsim 2$ TeV by the WMAP bound on relic density of LSP neutralino (red region). We can see from the $C-M_2$ panel that M_2 can be as low as 300 GeV. Such light M_2 solutions yield bino–wino mixing at the low scale which plays a role in reducing the relic abundance of LSP neutralino to the desired range. The $C-M_3$ plane shows that $M_3 \gtrsim 500$ GeV is compatible with QYU. This lower bound on M_3 is required by the heavy gluino mass constraint. Furthermore, solutions compatible with the WMAP require $M_3 \gtrsim 1.2$ TeV.

The results for the remaining parameters are shown in Fig. 2 with plots in $C-\tan\beta$ and $C-A_0/m_{16}$ planes. Color coding is the same as in Fig. 1. The $C-\tan\beta$ plane reveals that QYU requires rather high $\tan\beta$ values ($\tan\beta \gtrsim 56$), and the $C-A_0/m_{16}$ panel shows that A_0/m_{16} can lie in the range $(-2, 1)$.

We present the results for the mass spectrum of the colored sparticles and gluino in Fig. 3 in $m_{\tilde{q}}-m_{\tilde{g}}$, where $m_{\tilde{q}}$ denotes the masses of squarks of the first two families, and $m_{\tilde{t}}-m_{\tilde{\chi}_1^0}$ planes. Color coding is the same as in Fig. 1. In addition, the blue points satisfy $C \leq 0.2$ as well as QYU
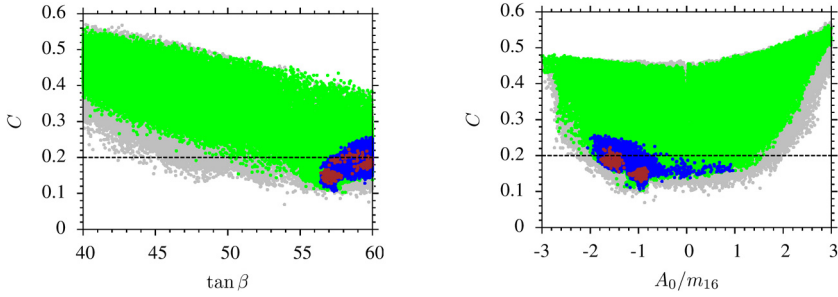
Fig. 2. Plots in C–$\tan\beta$ and C–A_0/m_{16} planes. Color coding is the same as in Fig. 1. (For interpretation of the references to color in this figure legend, the reader is referred to the web version of this article.)
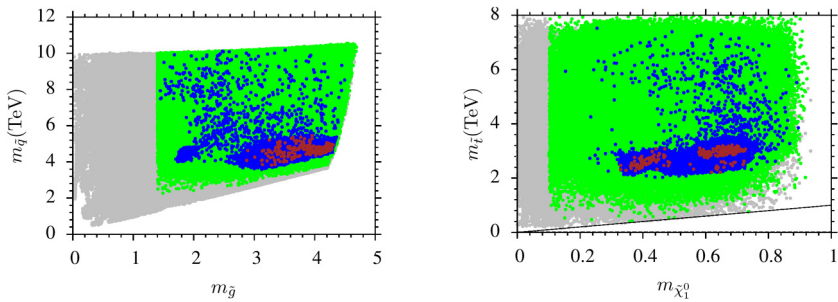

Fig. 3. Plots in $m_{\tilde{q}}$–$m_{\tilde{g}}$ and $m_{\tilde{t}}$–$m_{\tilde{\chi}_1^0}$ planes. Color coding is the same as in Fig. 1. In addition, the blue points satisfy $C \leq 0.2$ as well as QYU condition. (For interpretation of the references to color in this figure legend, the reader is referred to the web version of this article.)

condition. The gluino mass compatible with QYU and $C \leq 0.2$ is found to be $m_{\tilde{g}} \gtrsim 1.5$ TeV, and it can be tested in future experiments at the Large Hadron Collider (LHC). The squarks in QYU region are found to be of mass about 4 TeV. Similarly, the stop quarks satisfy $m_{\tilde{t}} \gtrsim 2$ TeV.

4. LSP neutralino and coannihilation scenarios

In the previous section we have focused on the fundamental parameter space and the mass spectrum of the colored particles. Since we accept only those solutions which lead to LSP neutralino, it is worth investigating the implications of 4-2-2 on the dark matter observables. In supersymmetric models with universal gaugino masses imposed at M_{GUT}, the LSP neutralino mostly happens to be Bino, and its relic abundance is usually so high that it cannot be consistent with the WMAP observation. However, one can identify various coannihilation channels that reduce the relic abundance of neutralino to the desired ranges. Since we allow nonuniversal gaugino masses determined by the 4-2-2 gauge group as given in Eq. (2), one can expect richer DM phenomenology. Indeed, 4-2-2 predicts various coannihilation channel scenarios at the low scale [10], but only the gluino–neutralino coannihilation scenario can survive if one imposes $t - b - \tau$ YU ($C = 0$) at M_{GUT} with $\mu > 0$ [7]. Relaxing this to $b - \tau$ YU opens up, in addition, the stop–neutralino channel [11]. In this section, we consider the phenomenological implications of QYU in 4-2-2 regarding the dark matter and the structure of LSP neutralino. Besides the bino-like LSP neutralino, it is possible to find solutions with bino–wino mixture, bino–higgsino mixture, or mostly higgsino LSP neutralino which leads to different phenomenology.
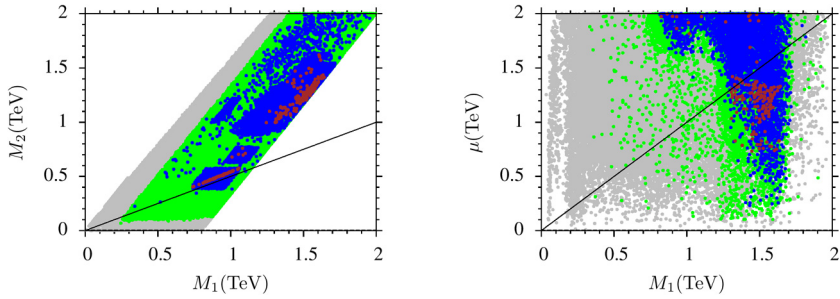
Fig. 4. Plots in M_2-M_1 and $\mu-M_1$ planes. Color coding is the same as in Fig. 3. (For interpretation of the references to color in this figure legend, the reader is referred to the web version of this article.)
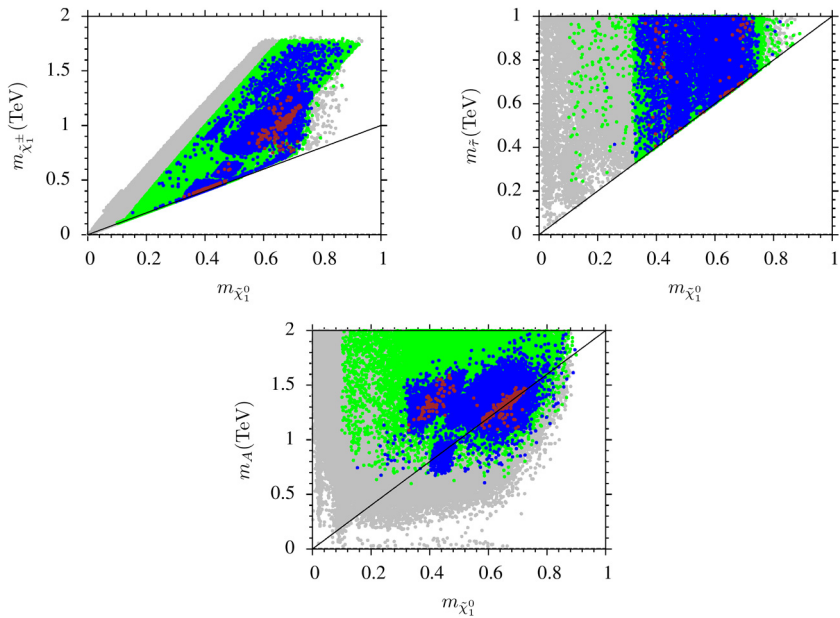

Fig. 5. Plots in $m_{\tilde{\chi}_1^\pm}-m_{\tilde{\chi}_1^0}$, $m_{\tilde{\tau}}-m_{\tilde{\chi}_1^0}$, and $m_A-m_{\tilde{\chi}_1^0}$ planes. Color coding is the same as in Fig. 3. The solid lines in the plots correspond to the related coannihilation channel regions. (For interpretation of the references to color in this figure legend, the reader is referred to the web version of this article.)

Fig. 4 displays the results in M_2-M_1 and $\mu-M_1$ planes. Color coding is the same as in Fig. 3. As stated in the previous section, M_2 can be as low as 300 GeV. The line in M_2-M_1 plane indicates solutions for which $M_1 = 2M_2$ and they yield bino–wino mixing at the low scale. Similarly, the line in $\mu-M_1$ plane corresponds to the solutions which have $M_1 = \mu$. These solutions can lead to very interesting implications, since LSP neutralino is bino–higgsino mixture near this line. Moreover, the LSP neutralino is found to be mostly higgsino below the line.

Fig. 5 summarizes our results for the coannihilation channels compatible with QYU in $m_{\tilde{\chi}_1^\pm}-m_{\tilde{\chi}_1^0}$, $m_{\tilde{\tau}}-m_{\tilde{\chi}_1^0}$, and $m_A-m_{\tilde{\chi}_1^0}$ planes. Color coding is the same as in Fig. 3. The solid lines in the plots correspond to the related coannihilation channel regions. Even though solutions in blue represent the regions compatible with QYU along with other LHC constraints, we rather
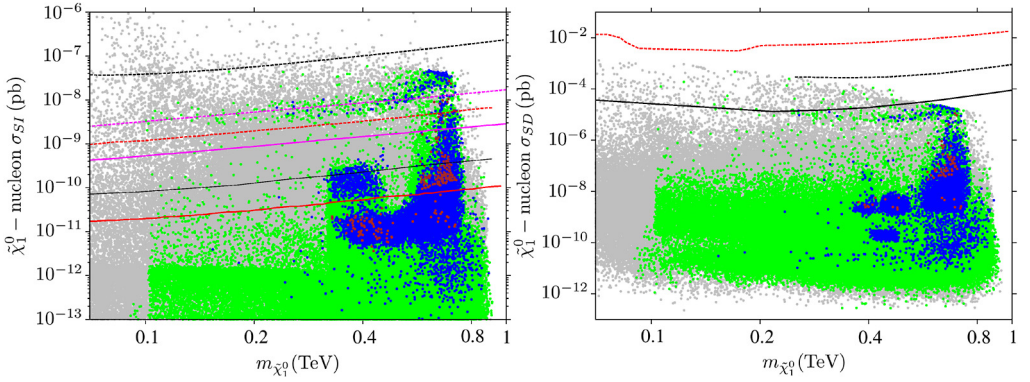
Fig. 6. Plots in $\tilde{\chi}_1^0$–nucleon σ_{SI} and $\tilde{\chi}_1^0$–nucleon σ_{SD} planes. Color coding is the same as in Fig. 3. In $\tilde{\chi}_1^0$–nucleon σ_{SI} plane, the dashed (solid) red line represents the current (future) bound from the XENON1T experiment [33], the dashed (solid) black line shows the current (future) bound of the CDMS [34] experiment, and the dashed (solid) magenta line displays the current (future) bound of the LUX experiment [35]. In $\tilde{\chi}_1^0$–nucleon σ_{SD} plane the dashed red line represents the bound from the Super K experiment, while the dashed (solid) black line shows the current (future) reach of the IceCube experiment. (For interpretation of the references to color in this figure legend, the reader is referred to the web version of this article.)

focus on the solutions in red, since these coannihilation channels reduce the relic density of LSP neutralino to the WMAP range such that the LSP neutralino can be identified as a pleasant candidate for the DM. The $m_{\tilde{\chi}_1^\pm} - m_{\tilde{\chi}_1^0}$ panel shows that the neutralino and the lightest chargino of mass $\gtrsim 300\,\text{GeV}$ can be nearly degenerate as expected from the $M_2 - M_1$ planes of Fig. 4. Besides chargino–neutralino coannihilation, the stau–neutralino channel is found to be compatible with QYU as seen from the $m_{\tilde{\tau}} - m_{\tilde{\chi}_1^0}$ plane, and stau can be as light as 400 GeV in this region. Another solution allowed by QYU is the A-resonance shown in the $m_A - m_{\tilde{\chi}_1^0}$ planes. The diagonal line in this panel corresponds to regions with $m_A = 2m_{\tilde{\chi}_1^0}$ in which two LSP neutralinos annihilate via the A-boson. The A-resonance solutions can be found for $m_{\tilde{\chi}_1^0} \gtrsim 600\,\text{GeV}$ and correspondingly $m_A \gtrsim 1.2\,\text{TeV}$ in the data set obtained.

5. Higgsino(-like) LSP

In the previous section we have identified various coannihilation channels and a resonance solution which reduce the relic abundance of LSP neutralino so that the dark matter phenomenology in the 4-2-2 framework can be consistent with the WMAP experiment. In this section we take a closer look at the structure of the LSP neutralino. Since the setup of 4-2-2 allows different kinds of LSP neutralinos such as bino–wino or bino–higgsino mixture, or mostly higgsino LSP, it opens up possibilities for direct detection experiments via relic LSP neutralino scattering on nuclei. When the LSP neutralino is mostly bino, it interacts with the quarks inside the nuclei only via the hypercharge, and hence the scattering crossection is too low to be tested in the direct detection experiments. On the other hand, the case with bino–wino mixture, or equivalently the one with chargino–neutralino coannihilation, yield moderate cross-sections in these scattering processes, since the LSP also interacts with quarks in the nucleon via $SU(2)$ interactions. The scattering cross-section reaches its highest values when the LSP neutralino is a bino–higgsino mixture or mostly higgsino, since the Yukawa interactions between quarks and the higgsino component of LSP neutralino take part in the scattering processes.

We present our results in Fig. 6 for neutralino–nucleon scattering for both the spin-independent and spin-dependent cases in $\tilde{\chi}_1^0$–nucleon σ_{SI} and $\tilde{\chi}_1^0$–nucleon σ_{SD} planes respectively. The color coding is the same as in Fig. 3. In the $\tilde{\chi}_1^0$–nucleon σ_{SI} plane, the dashed (solid) red line represents the current (future) bound from the XENON1T experiment [33], the dashed (solid) black line shows the current (future) bound of the CDMS [34] experiment, and the dashed (solid) magenta line displays the current (future) bound of the LUX experiment [35]. In the $\tilde{\chi}_1^0$–nucleon σ_{SD} plane, the dashed red line represents the bound from the Super K experiment, while the dashed (solid) black line shows the current (future) reach of the Ice-Cube experiment. As seen from the $\tilde{\chi}_1^0$–nucleon σ_{SI} plane, the spin-independent cross-section for the LSP neutralino with bino–wino mixture is of order 10^{-11} pb, while it rises by two orders of magnitude for bino–higgsino mixture. Furthermore, the spin-independent cross-section lies between 10^{-10}–10^{-8} pb if the LSP neutralino is mostly a higgsino, which is within reach of the direct detection experiments such as XENON1T, SuperCDMS and LUX. The red points placed between the dashed and solid lines of the same color are expected to be tested in the near future.

Before concluding, we want to highlight that the Higgsino(-like) dark matter can also be realized in the case of approximate universal gaugino masses. The plot in M_2–M_1 plane given in the left panel of Fig. 4 shows that the region with $M_2 \approx M_1 \approx 1.5$ TeV is consistent with the desired relic density of LSP neutralino. From the asymptotic gaugino mass relation given in Eq. (2), the approximate equality between M_1 and M_2 means $M_3 \approx M_1 \approx M_2$, and hence this region has the CMSSM-like boundary conditions. One can also identify this region in the μ–M_1 plane given in the right panel of Fig. 4. It can be seen that $\mu \lesssim M_1$ and hence this region predicts a Higgsino(-like) dark matter.

Finally, we present four benchmark points in Table 1 that exemplify the results obtained from our scans. The points are chosen to be consistent with the constraints mentioned in Section 2. Point 1 is an A-resonance solution, and point 2 depicts a solution with higgsino dark matter. Points 3 and 4 display stau–neutralino and chargino–neutralino coannihilation solutions respectively.

6. Conclusion

We have employed ISAJET to explore the LHC implications of Quasi-Yukawa unified (QYU) supersymmetric models based on the gauge symmetry $G = SU(4)_c \times SU(2)_L \times SU(2)_R$. In these QYU models, the third family Yukawa unification relations involving t, b and τ is quantified by a parameter C which takes values ~ 0.1–0.2. In contrast to earlier studies, the MSSM gaugino masses at M_{GUT} are non-universal but consistent with the gauge symmetry G. The thermal relic abundance of the LSP neutralino is compatible with the WMAP bounds through the chargino and stau coannihilation channels, as well as the A-resonance solution. These solutions predict stau mass(es) of about 400 GeV, and chargino mass of about 300 GeV which can be tested in colliders. We also identify solutions with Higgsino-like dark matter ($\mu \lesssim 1$ TeV), which can be tested in the direct dark matter searches such as XENON1T, SuperCDMS and LUX. The predicted gluino mass ranges from ~ 1.5–4 TeV, and the first two family squark masses are $\gtrsim 4$ TeV, which is consistent with the current gluino mass bound $m_{\tilde{g}} > 1.4$ TeV [29]. Similarly, one can consider the mass bounds on the stops which depend on the decay channels. If the stops decay into the LSP neutralino and the charm quark, the mass bound on the stop is about 270 GeV [36], and it rises to about 650 GeV if it decays into the LSP neutralino and bottom quark [37]. The mass bound on the stop is most severe, about 750 GeV, if it decays into

Table 1

Benchmark points exemplifying our findings. The points are chosen to be consistent with the constraints mentioned in Section 2. Point 1 is an A-resonance solution, Point 2 depicts a solution with the higgsino dark matter, the WMAP bound on relic abundance of LSP neutralino is satisfied through chargino–neutralino coannihilation for this point. Point 3 and Point 4 display stau–neutralino and chargino–neutralino coannihilation solutions respectively. Point 4 also exemplifies the solution with the heaviest CP-even Higgs boson mass we obtained.

	Point 1	Point 2	Point 3	Point 4
m_0	3362	3312	2905	3844
M_1	1343	1615	1436	893
M_2	1143	1407	1365	480.3
M_3	1643	1929	1542	1512
m_{10}	4058	4377	3332	4320
$\tan \beta$	57.1	57.2	57.4	59.7
A_0/m_0	−1.05	−0.94	−1.46	−1.74
m_t	173.3	173.3	173.3	173.3
μ	1420	752	2477	1996
m_h	123.1	123.4	123.8	124.7
m_H	1205	1126	1330	1394
m_A	1197	1118	1322	1385
$m_{H^\pm}$	1209	1130	1334	1397
$m_{\tilde{\chi}^0_{1,2}}$	595.8, 958.5	701, 766	639, 1150	397.2, 413.9
$m_{\tilde{\chi}^0_{3,4}}$	959.3, 1343	773, 1189	2000, 2003	2474, 2475
$m_{\tilde{\chi}^\pm_{1,2}}$	959.3, 1343	775, 1168	1151, 2003	414.5, 2476
$m_{\tilde{g}}$	3628	4174	3399	3408
$m_{\tilde{u}_{L,R}}$	4533, 4507	4860, 4816	4118, 4061	4726, 4737
$m_{\tilde{t}_{1,2}}$	2772, 3251	3044, 3517	2388, 2947	2395, 3053
$m_{\tilde{d}_{L,R}}$	4534, 4501	4861, 4816	4119, 4054	4726, 4737
$m_{\tilde{b}_{1,2}}$	3223, 3457	3489, 3670	2915, 3117	3028, 3459
$m_{\tilde{\nu}_{e,\mu}}$	3441	3434	3036	3854
$m_{\tilde{\nu}_\tau}$	2662	2647	2264	2750
$m_{\tilde{e}_{L,R}}$	3441, 3395	3434, 3362	3037, 2951	3854, 3856
$m_{\tilde{\tau}_{1,2}}$	1398, 2659	1293, 2644	650.7, 2263	405.6, 2748
σ_{SI}(pb)	0.13×10^{-9}	0.23×10^{-7}	0.26×10^{-10}	0.86×10^{-11}
σ_{SD}(pb)	0.43×10^{-7}	0.94×10^{-5}	0.56×10^{-8}	0.27×10^{-8}
Ωh^2	0.108	0.104	0.128	0.106
$y_{t,b,\tau}(M_{GUT})$	0.56, 0.41, 0.70	0.56, 0.44, 0.70	0.55, 0.38, 0.72	0.54, 0.37, 0.70
C	0.15	0.13	0.18	0.18

a LSP neutralino and top quark [38]. Despite such stringent bounds on the stop mass, the regions in which the stop is nearly degenerate with the top quark is not excluded. Moreover, these bounds are obtained with the assumption that the stop directly decays into the LSP neutralino and a quark. However, in our analysis the stop masses are heavier than 2 TeV, and they do not directly decay into LSP neutralino. In this sense, even if one does not impose the current LHC bounds on the mass spectrum by hand, the QYU condition automatically requires the current bounds.

Acknowledgements

References

[1] S. Dar, I. Gogoladze, Q. Shafi, C.S. Un, Phys. Rev. D 84 (2011) 085015, arXiv:1105.5122 [hep-ph].
[2] B. Ananthanarayan, G. Lazarides, Q. Shafi, Phys. Rev. D 44 (1991) 1613;
B. Ananthanarayan, G. Lazarides, Q. Shafi, Phys. Lett. B 300 (1993) 245;
Q. Shafi, B. Ananthanarayan, Trieste HEP Cosmol. (1991) 233–244.
[3] M.E. Gomez, G. Lazarides, C. Pallis, Nucl. Phys. B 638 (2002) 165, arXiv:hep-ph/0203131;
M.E. Gomez, G. Lazarides, C. Pallis, Phys. Rev. D 67 (2003) 097701, arXiv:hep-ph/0301064;
C. Pallis, M.E. Gomez, arXiv:hep-ph/0303098.
[4] J.C. Pati, A. Salam, Phys. Rev. D 10 (1974) 275.
[5] G. Lazarides, Q. Shafi, Nucl. Phys. B 189 (1981) 393;
S.F. King, Q. Shafi, Phys. Lett. B 422 (1998) 135, arXiv:hep-ph/9711288;
G. Lazarides, M. Magg, Q. Shafi, Phys. Lett. B 97 (1980) 87;
T.W. Kephart, C.A. Lee, Q. Shafi, J. High Energy Phys. 0701 (2007) 088, arXiv:hep-ph/0602055;
T.W. Kephart, Q. Shafi, Phys. Lett. B 520 (2001) 313, arXiv:hep-ph/0105237;
R.N. Mohapatra, J.C. Pati, Phys. Rev. D 11 (1975) 566;
G. Senjanovic, R.N. Mohapatra, Phys. Rev. D 12 (1975) 1502;
G. Senjanovic, Nucl. Phys. B 153 (1979) 334;
M. Magg, Q. Shafi, C. Wetterich, Phys. Lett. B 87 (1979) 227;
M. Cvetic, Nucl. Phys. B 233 (1984) 387;
T.W.B. Kibble, G. Lazarides, Q. Shafi, Phys. Lett. B 113 (1982) 237;
T.W.B. Kibble, G. Lazarides, Q. Shafi, Phys. Rev. D 26 (1982) 435;
R.N. Mohapatra, B. Sakita, Phys. Rev. D 21 (1980) 1062.
[6] C. Coriano, L. Delle Rose, C. Marzo, arXiv:1411.7168 [hep-ph].
[7] I. Gogoladze, R. Khalid, Q. Shafi, Phys. Rev. D 79 (2009) 115004, arXiv:0903.5204 [hep-ph].
[8] I. Gogoladze, Q. Shafi, C.S. Un, J. High Energy Phys. 1207 (2012) 055, arXiv:1203.6082 [hep-ph].
[9] I. Gogoladze, R. Khalid, S. Raza, Q. Shafi, J. High Energy Phys. 1012 (2010) 055, arXiv:1008.2765 [hep-ph].
[10] I. Gogoladze, R. Khalid, Q. Shafi, Phys. Rev. D 80 (2009) 095016, arXiv:0908.0731 [hep-ph].
[11] S. Raza, Q. Shafi, C.S. Ün, arXiv:1412.7672 [hep-ph].
[12] F.E. Paige, S.D. Protopopescu, H. Baer, X. Tata, arXiv:hep-ph/0312045;
For updates and changes in the current version, see, ISAJET 7.84.
[13] J. Hisano, H. Murayama, T. Yanagida, Nucl. Phys. B 402 (1993) 46;
Y. Yamada, Z. Phys. C 60 (1993) 83;
J.L. Chkareuli, I.G. Gogoladze, Phys. Rev. D 58 (1998) 055011.
[14] D.M. Pierce, J.A. Bagger, K.T. Matchev, R.j. Zhang, Nucl. Phys. B 491 (1997) 3, arXiv:hep-ph/9606211.
[15] ATLAS Collaboration, CDF Collaboration, CMS Collaboration, D0 Collaboration, arXiv:1403.4427 [hep-ex].
[16] I. Gogoladze, R. Khalid, S. Raza, Q. Shafi, arXiv:1402.2924 [hep-ph].
[17] I. Gogoladze, R. Khalid, S. Raza, Q. Shafi, J. High Energy Phys. 1106 (2011) 117.
[18] G. Belanger, F. Boudjema, A. Pukhov, R.K. Singh, J. High Energy Phys. 0911 (2009) 026;
H. Baer, S. Kraml, S. Sekmen, H. Summy, J. High Energy Phys. 0803 (2008) 056.
[19] L.E. Ibanez, G.G. Ross, Phys. Lett. B 110 (1982) 215;
K. Inoue, A. Kakuto, H. Komatsu, S. Takeshita, Prog. Theor. Phys. 68 (1982) 927;

K. Inoue, A. Kakuto, H. Komatsu, S. Takeshita, Prog. Theor. Phys. 70 (1983) 330 (Erratum);
L.E. Ibanez, Phys. Lett. B 118 (1982) 73;
J.R. Ellis, D.V. Nanopoulos, K. Tamvakis, Phys. Lett. B 121 (1983) 123;
L. Alvarez-Gaume, J. Polchinski, M.B. Wise, Nucl. Phys. B 221 (1983) 495.

[20] K. Nakamura, et al., Particle Data Group, J. Phys. G 37 (2010) 075021.
[21] R. Aaij, et al., LHCb Collaboration, Phys. Rev. Lett. 110 (2013) 021801.
[22] Y. Amhis, et al., Heavy Flavor Averaging Group, arXiv:1207.1158 [hep-ex].
[23] D. Asner, et al., Heavy Flavor Averaging Group, arXiv:1010.1589 [hep-ex].
[24] G. Hinshaw, et al., WMAP Collaboration, arXiv:1212.5226 [astro-ph.CO].
[25] H. Baer, M. Brhlik, Phys. Rev. D 55 (1997) 4463;
     H. Baer, M. Brhlik, D. Castano, X. Tata, Phys. Rev. D 58 (1998) 015007.
[26] K. Babu, C. Kolda, Phys. Rev. Lett. 84 (2000) 228;
     A. Dedes, H. Dreiner, U. Nierste, Phys. Rev. Lett. 87 (2001) 251804;
     J.K. Mizukoshi, X. Tata, Y. Wang, Phys. Rev. D 66 (2002) 115003.
[27] G. Aad, et al., ATLAS Collaboration, Phys. Lett. B 716 (2012) 1, arXiv:1207.7214 [hep-ex].
[28] S. Chatrchyan, et al., CMS Collaboration, Phys. Lett. B 716 (2012) 30, arXiv:1207.7235 [hep-ex].
[29] ATLAS Collaboration, ATLAS-CONF-2013-047.
[30] G. Degrassi, S. Heinemeyer, W. Hollik, P. Slavich, G. Weiglein, Eur. Phys. J. C 28 (2003) 133, arXiv:hep-ph/0212020;
     T. Hahn, S. Heinemeyer, W. Hollik, H. Rzehak, G. Weiglein, Phys. Rev. Lett. 112 (2014) 141801, arXiv:1312.4937 [hep-ph] and references therein.
[31] E. Kolb, M.S. Turner, The Early Universe, Frontiers in Physics, Addison Wesley, 1990.
[32] D.S. Gorbunov, V.A. Rubakov, Introduction to the Theory of the Early Universe, Moscow, URSS, 2008 (in Russian).
[33] E. Aprile, et al., XENON100 Collaboration, Phys. Rev. Lett. 109 (2012) 181301, arXiv:1207.5988 [astro-ph.CO],
     For the future projected sensitivity, see XENON1T 2017.
[34] J. Cooley, SuperCDMS Collaboration, AIP Conf. Proc. 1549 (2013) 223.
[35] M. Horn, et al., LUX Collaboration, Nucl. Instrum. Methods A 784 (2015) 504.
[36] ATLAS Collaboration, ATLAS-CONF-2013-068, ATLAS-COM-CONF-2013-076.
[37] V.I. Martinez Outschoorn, CMS Collaboration, EPJ Web Conf. 60 (2013) 18003.
[38] T. Lari, ATLAS Collaboration, PoS EPS-HEP2013 (2013) 294.